**HiSST: 2nd International Conference on High-Speed Vehicle Science Technology**
11–15 September 2022, Bruges, Belgium

# Feasibility Study for an Unmanned Re-entry Vehicle equipped with Deployable Wing System

*Roberto Fauci[1], Marco Marini[2], Francesco Di Caprio[3] Mario De Stefano Fumo[4], Pietro Catalano[5], Giovanni Andreutti[6], Antonio Schettino[7]*

## Abstract

The present paper summarizes the results of a feasibility study aimed at identifying a possible reference configuration of an unmanned space re-entry vehicle, class 2500 Kg (i.e. IXV, SPACE RIDER like), equipped with a deployable wing Sub-system. The activities have been performed in the framework of CIRA USV3 Deployable Wing System project. The scope of the project is the development of key technologies for future re-entry space vehicle configurations, enabling civil in-orbit experimentation, demonstration and scientific missions, with subsequent return from orbit, and finally safely landing for following refurbishment, and re-use. The main outcomes are discussed and in particular they refer to the aerodynamic and aerothermodynamic performance, concept design for deployable wing subsystem and thermal protection subsystems are presented.

**Keywords**: USV, *Re-entry, Deployable wing, Concept design*

## Nomenclature

**Latin**

| | |
|---|---|
| AEDB | aerodynamic data base |
| AFT-H | afterward hinge |
| APDL | Ansys Parametric Design Language |
| AoA | angle of attack |
| AoS | angle of sideslip |
| B | vehicle's wingspan |
| CA | axial force coefficient |
| CD | drag coefficient |
| CFD | computational fluid dynamics |
| CL | lift coefficient |
| CY | side force coefficient |
| Cl | rolling moment |
| Cm | pitching moment |
| Cn | yawing moment |
| CoG | center of gravity |
| DWS | Deployable wing system |
| ESA | European Space Agency |
| FRW-H | forward hinge |
| Ixx, Izz | inertia moments |
| L | vehicle's length |
| M | Mach number |
| MOGA | Multi objective genetic algorithm |
| Q | heat flux |
| QSL | quasi static load |
| PRR | Preliminary Requirement Review |
| Re | Reynolds number |
| S | surface |
| TPS | Thermal Protection System |
| USV | Unmanned Space Vehicle |

**Greek**

| | |
|---|---|
| α | angle of attack |
| β | angle of sideslip |
| δ | control surface deflection |

[1] *CIRA, Italian Aerospace Research Centre, Via Maiorise, 81043 Capua - Italy, r.fauci@cira.it*
[2] *CIRA, Italian Aerospace Research Centre, Via Maiorise, 81043 Capua - Italy, m.marini@cira.it*
[3] *CIRA, Italian Aerospace Research Centre, Via Maiorise, 81043 Capua - Italy, f.dicaprio@cira.it*
[4] *CIRA, Italian Aerospace Research Centre, Via Maiorise, 81043 Capua - Italy, m.destefano@cira.it*
[5] *CIRA, Italian Aerospace Research Centre, Via Maiorise, 81043 Capua - Italy, p.catalano@cira.it*
[6] *CIRA, Italian Aerospace Research Centre, Via Maiorise, 81043 Capua - Italy, g.andreutti@cira.it*
[7] *CIRA, Italian Aerospace Research Centre, Via Maiorise, 81043 Capua - Italy, a.schettino@cira.it*

 

| **Subscripts** | | | |
|---|---|---|---|
| α | α-derivative | f | flaperon, friction |
| β | β-derivative | i | inviscid |
| base | related to baseplate | ref | reference |
| bf | body-flap | st | stabilator |
| | | wet | wetted |

## 1. Introduction

The Italian Aerospace Research Centre (CIRA) was the prime contractor on the national aerospace research program, named PRO.R.A. In such context, CIRA is involved in the "USV-Unmanned Space Vehicle" project, whose main objective is the development of technologies, materials, and systems for future unmanned space re-entry vehicle. Again, after the successful heritage of the IXV program [1] CIRA is now deeply involved in ESA Space Rider Program, having in charge the design, development and procurement of the Ceramic Thermal Protection Systems, including also the control surfaces [2]. CIRA is also prime contractor for the Space Rider Drop test.

In this framework, the idea pursued in the context of the so called USV3 DWS (Deployable Wing System) project is to investigate the feasibility of a re-entry vehicle equipped with fins, elevons and/or body flaps and capable of performing safely a controlled return and a conventional landing using a deployable wing. Reference system is a class 2500 Kg re-entry vehicle (i.e. USV3, IXV, SPACE RIDER like), to be launched by using Italian VEGA C launcher.

Re-entry winged body vehicles (i.e. USV3 like) have several advantages w.r.t capsules/lifting bodies (i.e. Space Rider like), such as maneuverability and controlled landing opportunity. On the other hand, they show an increment in design level complexity, especially from an aerodynamic, aero-thermodynamic and structural point of view, and in the difficulties of housing in operative existing launchers. In this framework, the idea of designing unmanned vehicle equipped with deployable wings for suborbital flight was conceived.

## 2. Trade-off analysis for Concept configuration and aero-shape selection

The selected vehicle concept configuration equipped with a deployable wing is the output of a trade-off study (phase 0/A study) that aimed to define a possible system concept design and related high-level system requirements, considering the following criteria: global weight minimization; payload maximization; optimization of aerodynamic efficiency over all the flight regimes; mass minimization of wing thermal shields; maximization of mechanisms' simplicity and reliability. In particular, two different concepts, each one with a different re-entry strategy, have been identified and analyzed by exploiting the experience acquired during USV and IXV programs and the ongoing activity on the Space Rider European program.

The first concept ("capsule based") is expected to operate a re-entry mission based on the following three phases: atmospheric re-entry without wing (lifting body) and controlled flight up to the low supersonic or transonic regime; deceleration using a parachute (if needed) and deployment of the wing; controlled flight through transonic and subsonic regimes up to landing. The concept is "IXV derived", simply obtained by applying wings to the "lifting body" and slightly modifying the fuselage in order to accommodate the "undeployed" wing, so that no critical thermal effect should occur on the wings during the first re-entry phase.

| **Criteria** | **Configurations** | | |
|---|---|---|---|
| | LB1 (top wing) | **LB2 (medium wing)** | LB3 (low wing) |
| | 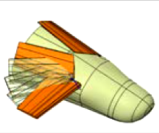 |  | 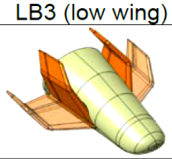 |
| Minimum thermal shield | Very good | Good | Discrete |
| Aerodynamic performance | Very low | Discrete | Discrete |
| Space for stowed configuration | Very good | Good | Discrete |
| Mechanism flexibility & reliability | Good | Discrete | Discrete |

**Fig 1.** USV3 DWS "capsule based" concept configurations comparison vs selected criteria

 

For this concept, different configurations, foreseeing solutions with a "top" wing, "medium" wing and "low" wing have been conceived and compared each other (evaluation results are shown in Fig 1). The performed investigation has led to the selection of the so called "LB2" configuration as the most applicable one [3].

The second concept (USV3 "wing body" based) is designed to operate a re-entry mission performing a wing deployment prior to the atmospheric re-entry and to operate all the aerodynamic regimes with a "winged" configuration. The vehicle has been equipped with fins, elevons and a body-flap.

Starting point has been the conclusion of a first trade-off study performed in the framework of the USV3 PRIDE project [4]. The analysis was conducted through a Multi Criteria Decision-Making process (MCDM) based on "ranked" evaluation criteria, determining the conclusion showed in Fig 2.

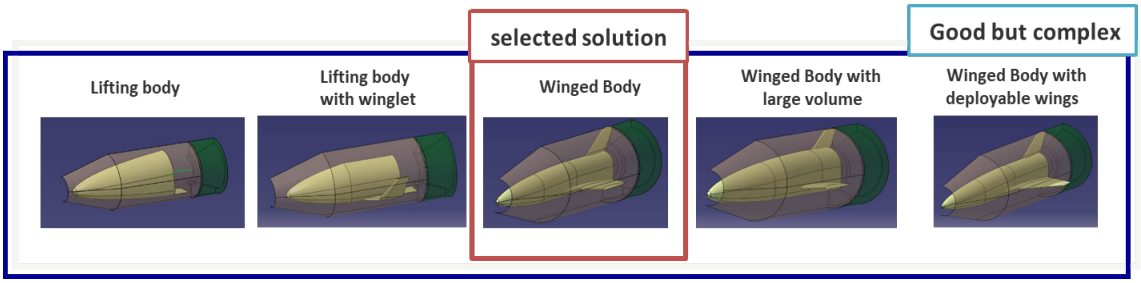


**Fig 2.** Lifting body vs Wing body configuration trade off analysis

The previous analysis showed the potentiality of a configuration with deployable wings, especially in terms of aerodynamic performance, despite its complexity. For this concept, it was decided to investigate a configuration having the portion of wing to be deployed as large as possible, both for fitting the winged vehicle into the VEGA C fairing and for avoiding the adoption of very stretched configurations, as made for previous configuration of USV3. Different configurations (see Fig 3) have been analyzed in terms of aerodynamic performances by varying the wing profile shape, wing longitudinal position, angular deflection of fins composing the vertical tail (V-tail), etc. Some results at landing phase are summarized in Table 1. The best one is the configuration 8 (C8 in the following).

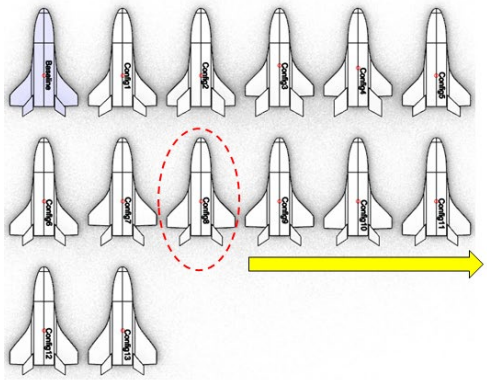

| Configuration | Fuselage | Wing | Vtail | CoG |
|---|---|---|---|---|
| Baseline | baseline | baseline | Baseline Γ=45° | 68% length |
| Config1 | baseline | baseline | Baseline Γ=30° | 68% length |
| Config2 | baseline | baseline | Mid Γ=30° | 68% length |
| Config3 | baseline | shift fw 530 mm | Mid Γ=30° | 68% length |
| Config4 | baseline | shift fw 530 mm | Mid Γ=30° | 60% length |
| Config5 | baseline | αtw = 0° | Baseline Γ=45° | 68% length |
| Config6 | baseline | baseline | Baseline Γ=45° | 65% lenght |
| Config7 | baseline | shift fw 530 mm | Baseline Γ=45° | 65% lenght |
| Config8 | baseline | shift fw 406 mm | Baseline Γ=45° | 65% lenght |
| Config9 | baseline | shift fw 453 mm | Baseline Γ=45° | 65% lenght |
| Config10 | baseline | shift fw 358 mm | Baseline Γ=45° | 65% lenght |
| Config11 | baseline | +10% chord | Baseline Γ=45° | 65% lenght |
| Config12 | baseline | +20% chord | Baseline Γ=45° | 65% lenght |
| Config13 | baseline | +30% chord | Baseline Γ=45° | 65% lenght |

**Fig 3.** USV3 DWS Wing body Concept configurations comparison - reference parameters

**Table 1.** Wing based most promising configuration - Landing parameters comparison

| Configuration | AoA_trim (°) | CL_land | δf (°) | δst (°) | S.M. (%) |
|---|---|---|---|---|---|
| Baseline | 17.21 | 0.45 | -20 | -18.48 | 3.83 |
| **Config8** | **16.32** | **0.45** | **-20** | **-12.01** | **2.04** |
| Config9 | 16.12 | 0.45 | -20 | -9.27 | 1.52 |
| Config13 | 15.90 | 0.45 | -20 | -6.90 | 2.63 |

In terms of the deployment mechanism, the first concept is, of course, more demanding, from a structural point of view, due to the fact that the deployment happens in the atmosphere and, therefore,

the actuation system can withstand the aerodynamic forces and be quickly executed to guarantee a significant synchronization level in the wings deployment phase. Further, some mechanism components would be exposed for a long time to the space environment during the orbital phase. These issues are avoided for the second concept, because the wing releasing phase occurs at the beginning of the orbital phase. On the other hand, the mechanism components of the second concept shall be designed considering the presence, on the wing, of a significant thermal protection system (TPS) layer, reducing the available clearance for mechanism housing and requiring significant wing design efforts for guaranteeing both TPS housing and wing aerodynamic performance.

## 3. Baseline configuration – Layout and Preliminary mass budget

At the end of the trade-off analysis, a configuration based on the wing deployment at the beginning of the orbit phase was defined as the best one. Fig 4 shows the selected configuration, identified as USV3 DWS "WB-B3-C8" in operative condition (deployed wings) and in stored configuration inside the schematic VEGA-C fairing (folded wings).

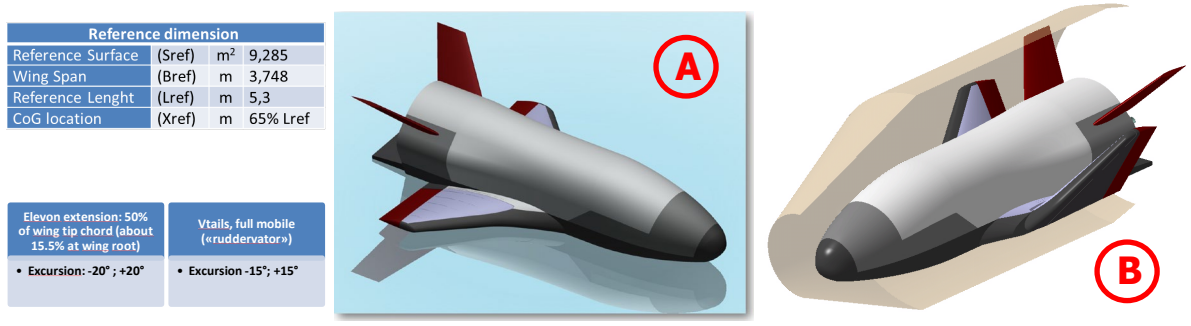


**Fig 4.** A: USV3 DWS configuration - wing deployed; B: stored configuration inside the schematic VEGA-C fairing

Physical internal architecture has been defined taking in account the heritage of IXV, USV3 and Space Rider project, and assuming that the identified sub-systems for the new concept are the same and have the same functionality, due to the fact that the orbital and re-entry mission phases are, more or less, equal.

In detail, with the exception of DWS and TPS sub-systems, solutions already defined for USV3-Pride and/or IXV have been adopted. Also, the cold structure has been slightly revised in order to match modified fuselage shape, new wing location, wing shape including elevons, presence of vertical tails, payload bay location. Anyway, design philosophy and material choice (Ti-6Al-4V) have been kept. Fig 5 show WB-B3-C8 the configuration internal layout, the high-level product tree and the preliminary mass budget.

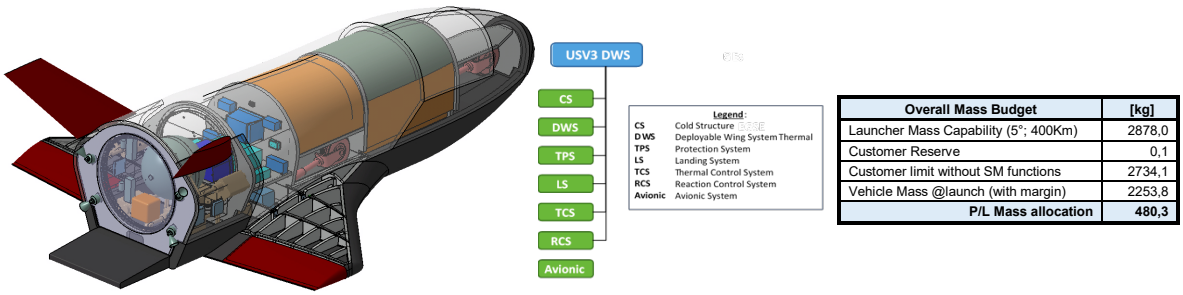


| Overall Mass Budget | [kg] |
|---|---|
| Launcher Mass Capability (5°; 400Km) | 2878,0 |
| Customer Reserve | 0,1 |
| Customer limit without SM functions | 2734,1 |
| Vehicle Mass @launch (with margin) | 2253,8 |
| **P/L Mass allocation** | **480,3** |

**Fig 5.** WB-B3-C8 configuration internal layout, main product tree and preliminary mass budget

## 4. Aerodynamic and aerothermodynamic database

### 4.1. Aerodynamic Database Development

Once the final configuration was identified, the aerodynamic database (AEDB) has been developed to provide data for flight mechanics analysis (stability, trim-ability, controllability, etc.) and nominal flight trajectory calculation starting from mission requirements. The classical Space-Based approach has been

 

followed in which the aerodynamic coefficients (CL, CD, CY, Cl, Cm, Cn) are function of independent variables describing flight conditions (Mach, Re or altitude) and vehicle's attitude (AoA, AoS, $\delta_f$, $\delta_{st}$, $\delta_{bf}$); moreover, also an uncertainty model for aerodynamic coefficients is typically given, but this is out of the present work.

The development of AEDB from subsonic to low supersonic regime (Mach=2) is based on detailed CFD simulations in turbulent regime for clean configuration, with corrections due to control surfaces deflection computed by engineering methods. For supersonic-to-hypersonic regime (from Mach=2 to Mach=25), the AEDB development is based on surface impact methods only (both clean and deflected configurations) with baseflow and viscous effects evaluated by engineering formulas. In the aerodynamic reference system here adopted, the conditions for longitudinal and lateral-directional aerodynamic stability are reported in Table 2

**Table 2.** conditions for longitudinal and lateral-directional aerodynamic stability

| | |
|---|---|
| Longitudinal static stability | $Cm_\alpha < 0$ |
| Side force static stability | $CY_\beta < 0$ |
| Roll static stability | $Cl_\beta < 0$ |
| Yaw static stability | $Cn_\beta > 0$ |
| Roll-yaw coupling dynamic stability | $Cn^*_\beta = Cn_\beta cos\alpha - \frac{I_{zz}}{I_{xx}} Cl_\beta sin\alpha > 0$ |

### 4.2. Subsonic-Transonic-Low Supersonic Regime

The aerodynamic characterization of the USV3-DWS WB-B3-C8 aeroshape from subsonic to low supersonic regime has been done using a mixed approach CFD/engineering method with the following specifications:

- Clean Configuration
- CFD Navier-Stokes fully turbulent simulations [5][6][7]on structured grids (see Fig 6)
- Mach=0.3, 0.6, 0.8, 0.95, 1.2, 1.4, 2.0
- AoA=0°, 5°, 10°, 15°, 20°, 25°
- AoS=0°, 4° (not for all AoAs)
- Reynolds effect at Mach=0.6, 0.95 and 2, AoA=10°, AoS=0°
- Control surfaces deflection computed by engineering methods with viscous correction [8], with anchoring/tuning to CFD aerodynamic coefficients computed for clean configuration):
    - Body-Flap ($\delta_{bf}$) =-40°, -30°, -20°, -10°, 0°, 10°, 20° (solo Mach=2)
    - Flaperon ($\delta_f$) =-20°, -15°, -10°, -5°, 0°, 5°, 10°, 15°, 20°
    - Stabilator ($\delta_{st}$) =-30°, -25°, -20°, -15°, -10°, -5°, 0°, 5°, 10°, 15°, 20°, 25°, 30°

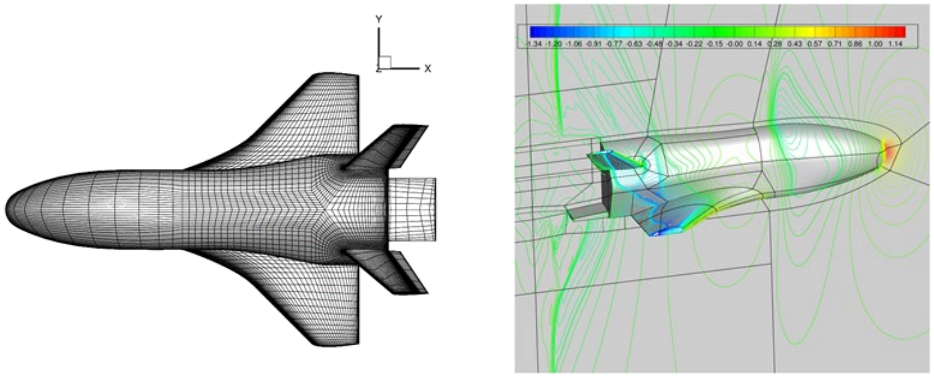

**Fig 6.** Surface grid (left) and Cp contours around the vehicle for M=0.95, AoA=5° (right)

The longitudinal aerodynamics of the clean vehicle is shown in Fig 7, where CL, CD and Cm in function of AoA are reported for Mach number ranging from 0.3 to 2.

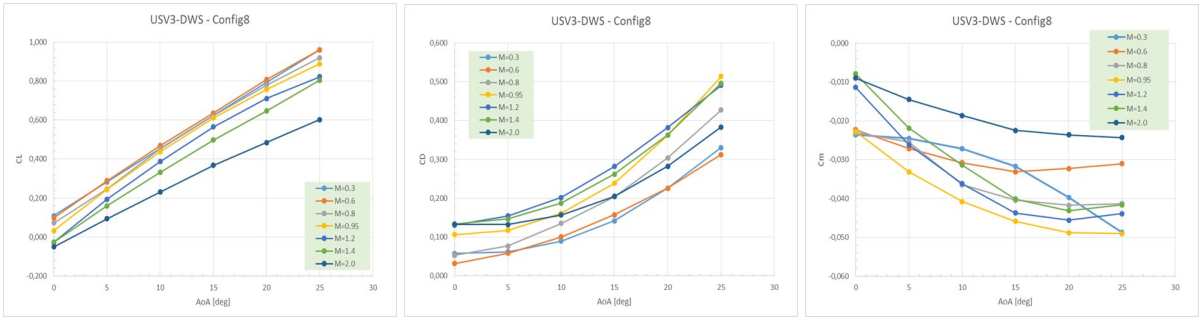


**Fig 7.** CL (left), CD (middle) and Cm (right) in function of AoA

From Fig 7 it can be observed the quasi-linear behaviour of CL with AoA, the maximum CD between Mach=1.2 and 1.4, and the maximum lift-to-drag ratio (~5) for Mach=0.3 and AoA=10°, i.e. in conditions very close to landing; moreover, the longitudinal stability ($Cm_\alpha<0$) is assured for all Mach numbers up to AoA=15°÷20°. The Reynolds number (i.e. altitude) effect on aerodynamic coefficients has been described by means of second order polynomials, basing on detailed CFD simulations at Mach=0.6, 0.95, 2.

For what concerns lateral-directional stability, it has been predicted a side force ($CY_\beta<0$) and roll ($Cl_\beta<0$) static stability for all Mach numbers and AoAs considered, whilst a clear yaw static instability ($Cn_\beta<0$) is observed for all investigated cases. The dynamic stability has been preliminarily studied for the roll-yaw coupling (see paragraph 4.1) parameter $Cn_\beta$* dynamic, analyzing parametrically the effect of inertia moments ratio (Izz/Ixx=4, 6, 8) the goal being to determine for each Mach number the critical AoA for roll-yaw coupling. Results (not shown here for sake of brevity) indicate that a greater ratio Izz/Ixx means a greater lateral-directional dynamic stability, i.e. is lower the critical AoA at which the $Cn_\beta$* dynamic condition is violated, this latter condition affecting the AoA profile in function of Mach number. As an example, for the more realistic case of Izz/Ixx=4 the $Cn_\beta$* dynamic condition indicates that at landing (Mach=0.3) the angle of attack must be AoA>8.2°.

The analysis of the complete AEDB, including the effect of control surfaces (deflection of flaperon, $\delta_f$, and of stabilator, $\delta_{st}$), has resulted in a preliminary identification of trim conditions decreasing Mach number along the descent to landing, as shown in Fig 8 left. To trim the vehicle the use of most of flaperon deflection range is necessary, with the stabilator set at full-range, especially during the phase approach and landing. For the landing condition (Mach=0.3, velocity 102.08 m/s) the trim condition identified from AEDB provides a CL=0.4826, so slightly higher than CL=0.4525 as defined as target for a landing weight of 2734 kg, see Fig 8 right.

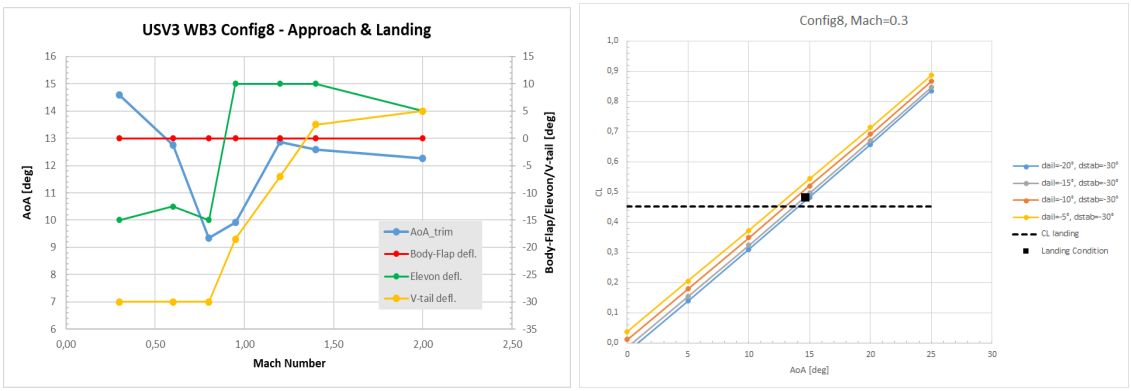


**Fig 8.** Trim conditions in approach and landing phase (left) and landing conditions (right)

### 4.3. Supersonic-Hypersonic Regime

The aerodynamic characterization of the selected configuration from supersonic to hypersonic regime has been elaborated using an engineering method with the following specifications:

 

- Clean Configuration
- Simulations with Surface Impact Methods (VECC, [9]) on surface grids
- Inviscid flow
- Mach=2, 3, 4, 6, 10, 15, 20, 25
- AoA=0°, 5°, 10°, 15°, 20°, 25°, 30°, 35°, 40°, 45°, 50°
- AoS=0°, 2°
- Control surface deflections:
  - Body-Flap ($\delta_{bf}$) =-40°, -30°, -20°, -10°, 0°, 10°, 20°
  - Flaperon ($\delta_f$) =-20°, -15°, -10°, -5°, 0°, 5°, 10°, 15°, 20°
  - Stabilator ($\delta_{st}$) =0°

For each part of the vehicle the more proper engineering method to compute pressure distribution has been selected. For the baseplate, a correction has been added to axial force coefficient, i.e.

$$CAbase = \frac{1}{M^2} * \frac{Sbase}{Sref}$$

where the baseplate surface of the USV3-DWS WB-B3-C8 vehicle is equal to $S_{base}$=1.56 m$^2$.

The correction for viscous effects is estimated through an engineering correlation to be applied along the calculation of the flight path, as a function of altitude. The viscous correction is applied only to the axial force ($CA = CA_i + CA_f$), assuming the vehicle can be assimilated to a flat plate whose wetted area (Swet) is equivalent to the planform area of the vehicle. With this assumption, the friction coefficient is evaluated with the modified Schlichting correlation [10], that is:

$$C_f = \frac{0{,}42}{\left(log_{10}\left(Re_{Lref}\right)\right)^{2{,}55}\left(1 + 0{,}25M_{\infty}^2\right)^{0{,}31}}$$

where ∞ indicates free stream conditions and $CA_f=C_f \cdot S_{wet}/S_{ref}$.

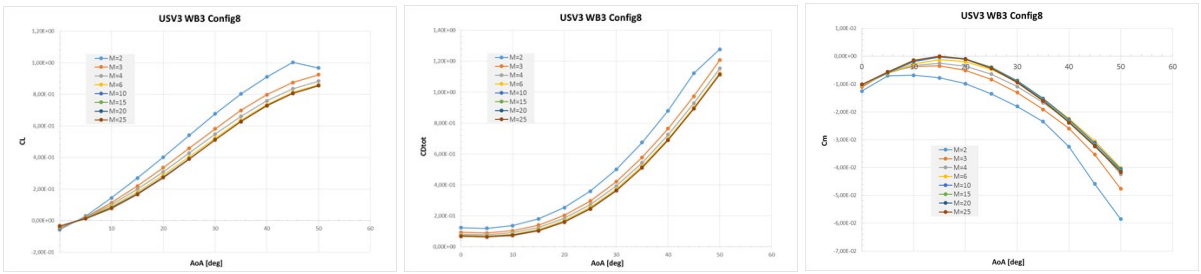


**Fig 9.** CL (left), CD (middle) and Cm (right) in function of AoA

The longitudinal aerodynamics predicted for the clean configuration is reported in Fig 9, where CL, CD and Cm are shown in function of AoA for Mach ranging from 2 to 25. There is a "not very linear" trend of the lift coefficient CL in the whole range of AoA considered (from 0° to 50°), and above all a negative CL for AoA=0 ° at all the Mach numbers considered, while the maximum value of the drag coefficient CD (classic quadratic trend with AoA) is observed at Mach=2. The maximum aerodynamic efficiency (equal to about 2) is also observed at Mach=2 with a peak at AoA≈15°, while the longitudinal static stability ($Cm_\alpha$ <0) is ensured at all Mach numbers for AoA>15°.

For what concerns lateral-directional stability, it has been predicted a side force static stability ($CY_\beta$<0) for all Mach numbers and AoAs considered, a roll static stability ($Cl_\beta$<0) 0 for all Mach numbers and AoA>15°, whilst a clear yaw static instability ($Cn_\beta$<0) is predicted for all investigated conditions.

As far as dynamic stability (roll-yaw coupling, $Cn_\beta$*>0) is concerned, results (not shown here) indicate that a greater ratio Izz/Ixx means a greater lateral-directional dynamic stability, i.e. is lower the critical AoA at which the $Cn_\beta$* dynamic condition is violated, this latter condition affecting the AoA profile in

function of Mach number. As an example, for the more realistic case of Izz/Ixx=4 the $Cn_\beta$* dynamic condition indicates that at Mach=25 the angle of attack must be AoA>28.92° while at Mach=2 it must be AoA>31.12°.

A first analysis of the possible trim conditions of the vehicle during re-entry was first made by evaluating only the effect of the deflection of the body-flap ($\delta_{bf}$=-40°÷0°) on the Cm, in the hypothesis of non-deflected flaperon ($\delta_f$=0°), and then considering for the lower values of the Mach number the combined effect of body-flap ($\delta_{bf}$=-10°) and flaperon. This first fly-ability analysis, focused to stability and trim-ability in supersonic-hypersonic regime, produced two possible re-entry corridors in the hypothesis of USV3-DWS WB3 with Izz/Ixx=4 and longitudinal flight (AoS=0°): i) corridor#1 with use of body-flap only (from -40° to -20°) e flaperon=0°, and ii) corridor#2 with use of body-flap (from -40° to -10°) and flaperon<0° for Mach number lower than 4. Corridor#1 was characterized by a dynamic instability at Mach=2, while for corridor#2 the combined use of body-flap and flaperon eliminated the possibility of having dynamic instability up to Mach=2.

### 4.4. Preliminary Analysis of Re-entry Corridor

A first analysis about the stability and trim-ability of the USV3-DWS WB-B3-C8 vehicle, basing on the full AEDB obtained properly joining the subsonic-transonic-low supersonic branch to the supersonic-hypersonic one, has allowed to preliminarily define a (nominal) complete re-entry corridor, from Mach=25 down to landing at Mach=0.3, see Fig 10.

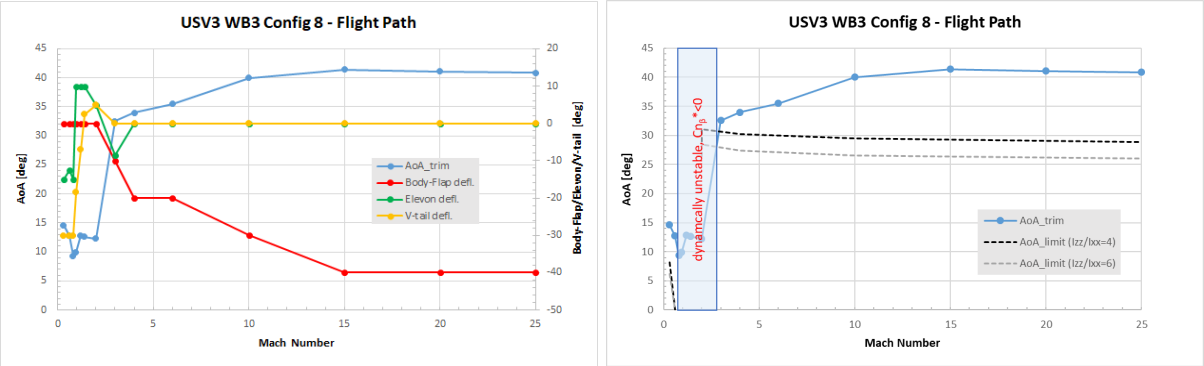


**Fig 10.** Re-entry corridor in terms of di AoA, $\delta_{bf}$, $\delta_f$, $\delta_{st}$ (left) and AoA with dynamic stability conditions $Cn_\beta$*>0 (right) in function of Mach number

The strategy followed along this preliminary re-entry corridor foresees an angle of attack around 40° with body-flap negatively deflected down to Mach=10, then AoA and $\delta_{bf}$ are reduced whereas start the activation of flaperon (at Mach=3) and stabilator (at Mach=2). From this point on the body-flap is undeflected and the vehicle is controlled with a combination of flaperon and stabilator deflections down to landing. As far as dynamic stability condition ($Cn_\beta$*>0) is concerned, from the analysis of results it emerges that the vehicle with inertia moments ratio Izz/Ixx=4 is stable down to Mach=3 and for Mach number lower than 0.8, so also in landing conditions. Instead, a region of dynamic instability is identified during the final part of the re-entry below Mach=3 and up to Mach=0.8.

### 4.5. Aerothermodynamic Database Development

The heat fluxes to the vehicle USV3-DWS WB-B3-C8 have been computed by using the engineering method (VECC, [9]) and verified with some CFD simulations along a USV3 reference trajectory. Particular attention has been given to provide results obtained with the same hypotheses (no real gas effects, same wall temperature) and which are conservative for some critical regions of the vehicle.

The comparison of results provided by engineering method and CFD is shown in Fig 11 for the condition of maximum heat flux along the USV3 reference trajectory (T-03 case). The heat flows predicted by VECC are generally greater than the CFD results, and also some three-dimensional effects are obviously not "captured" by the engineering method. For the wing, only the heat flux values at wing tip are shown, the highest, which are therefore the sizing ones for the wing itself.

 

Two approaches have been developed for sizing heat fluxes database: i) direct use of values computed by VECC (along relevant streamlines) or ii) use of CFD results of T-03 case properly scaled along the trajectory, i.e.

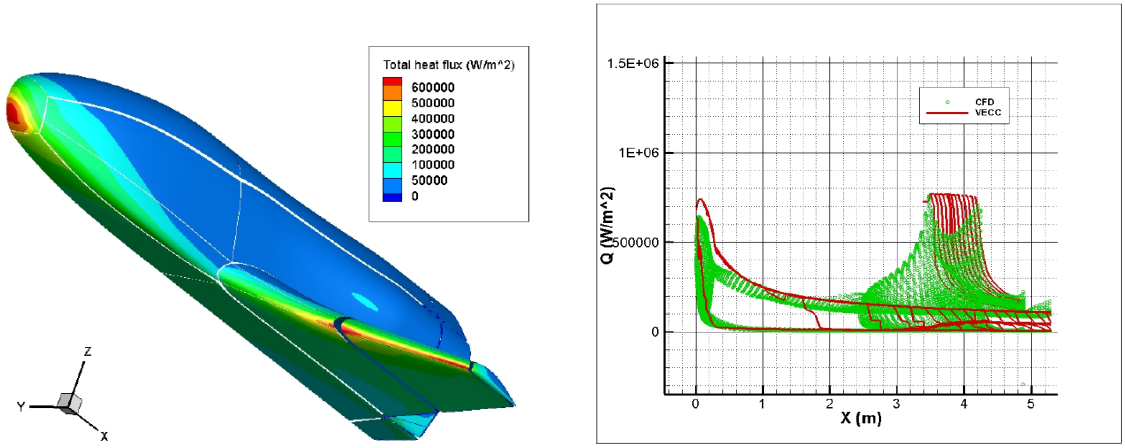


**Fig 11.** Heat flux CFD results (left) and comparison CFD/VECC (right) for Mach=21.84, AoA=37.42°, altitude=73.94 km

## 5. Deployable wing system concept definition

### 5.1. Concept definition

The DWS concept design definition started by a state-of-the-art study, covering both aeronautical and aerospace application and showing that, notwithstanding the literature proposes a huge number of patents that have been achieved especially by US scientists and companies, forecasting visionary solutions to be applied to space re-entry systems, there are very few real examples of spacecraft with deployable wings. Anyway, in terms of both mission and deployment system, similarity with the USV3 DWS vehicle can be found in the orbital stage of the Soviet Spiral vehicle, in the proto flight Vehicle 201 (developed in the framework of the X38 program) [11] and in the Dream Chaser Cargo System (unmanned variant of the Dream Chaser Space System). Other references belong to the distribution of solar panel arrays, that could have similarity with the DWS since the USV3 DWS deployment takes place outside the atmosphere.

For this concept, it has been decided to have the deployable wing section as bigger as possible in order to be allocated in the VEGA C fairing. The rotational axis has been defined taking into account the need both to minimize the portion of fixed wing and to minimize the gap between fixed wing portion and deployable wing, avoiding any interference during the deployment operations. The fuselage interface is represented by two hinges, named respectively FRW-H (FoRWard Hinge) and AFT-H (AFTerward Hinge). The locking subsystem is made up of a set of pins, moved each one by a linear actuator that has the purpose of retracting the pin (release function) before the deploying phase, and re-inserting the pins into their seats when the deployment phase is completed (Fig 12).

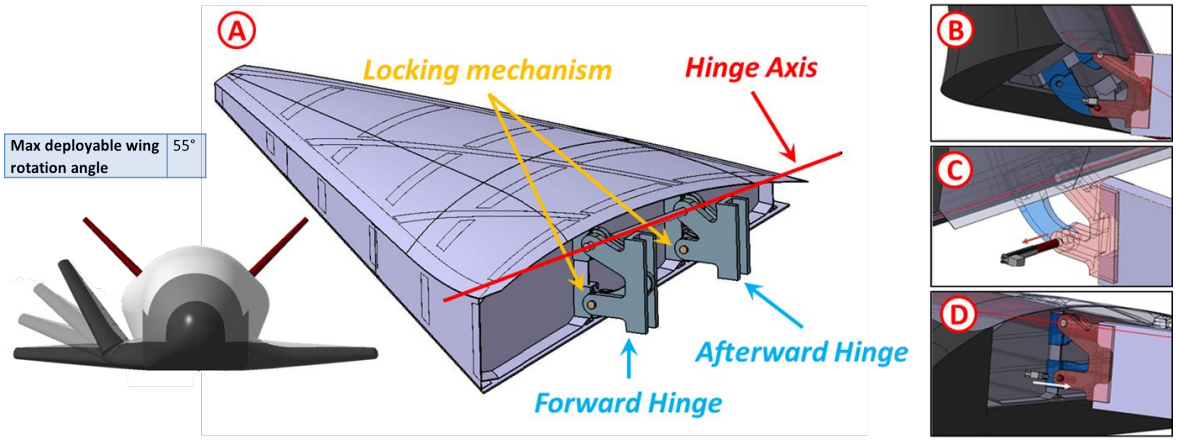

**Fig 12.** A: Wing model with schematic hinges; B: Wing undeployed and locked; C: Wing undeployed and unlocked; D: wing deployed and locked

### 5.2. Design Optimization of Interfacing Attachments

The definition of the best design for the hinges foresees as a first step the evaluation of the interface loads. After having determined the latter, it will be possible to design and optimize the shapes of the hinges. Obviously, the lower the interface forces, the lower the structural mass of the hinges will be, considering already defined the mechanical properties of the materials to be used. The study aims to determine the best hinges position such as to minimize the interface forces, in both configurations (unfolded and folded) [12]. A simplified Finite Element (FE) parametric model was defined in the ANSYS environment. The FE model allows to evaluate more accurately the hinges position and, above all, any interference with the main structure.

For each configuration a specific set of load conditions was considered. In the deployed configuration the load, equal to 13.6 kN, works along the vehicle Z axis, and it has been applied at the pressure center. For the folded configuration, i.e. when the vehicle is placed in the fairing of VEGA-C, the load derives from the accelerations field generated by the launch phases and they can be schematically applied at the center of gravity of the wing (CoG). In such case the worst quasi static loads (QSL) combination was considered, i.e. -7.5 g along longitudinal direction and 1.35g along later directions (vehicle axis) [13].

Fig 13 shows the model in both configurations and in particular the main axes are highlighted (hinge axis, stopper axis in folded and deployed configuration). It is important to underline that the real position of the interfacing point depend upon such axes.

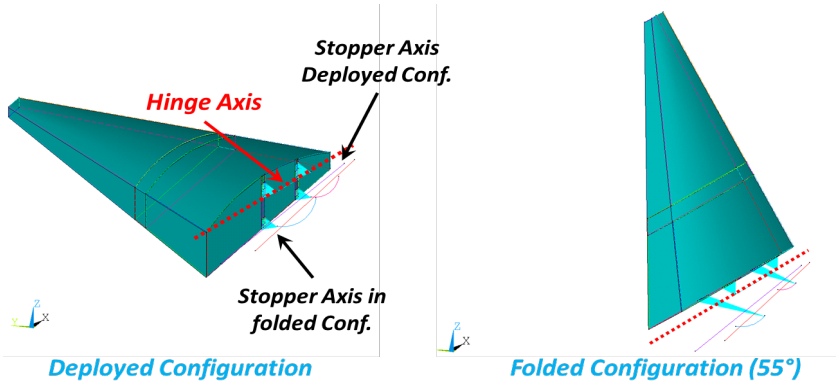


**Fig 13.** Adopted Simplified Numerical model in deployed and folded configuration

The positions of the hinges are defined by means of four parameters that represent the design variables of the optimization problem. The points location is defined by four parameters: the position along the X-axis of C1 and C4 points (H1-X and H2-X) and the position along the Z-axis of points C2 and C5 (H1-Z and H2-Z) as reported in Fig 14. Points C3 and C6 are automatically determined by defining the wing rotation angle by a rigid rotation of C2 and C5 points around the Hinge axis (Fig 14).

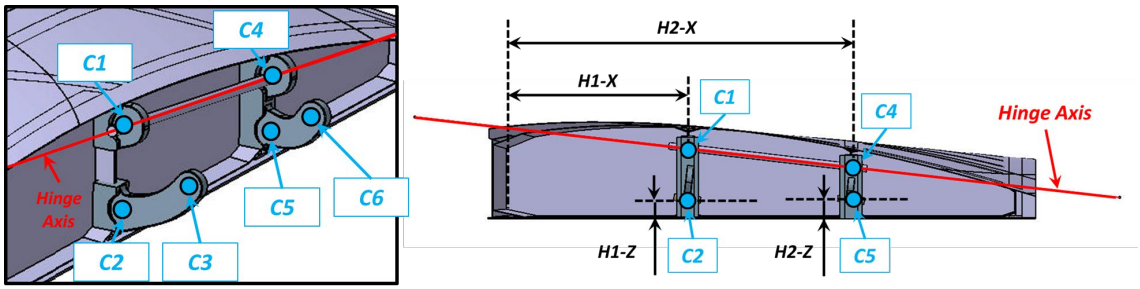


**Fig 14.** design variable definition (hinges position)

The ANSYS model was implemented in a Mode-Frontier [14] optimization workflow, thus an APDL macro is able to generate, on demand, any configuration defined by optimization tool. A multi objective genetic algorithm (MOGA-II) was used and the initial generation was defined using a SOBOL algorithm with 30 individuals. The entire process last ten generation, therefore at the end 300 individuals will be evaluated.

The output variables are the bearing and axial forces (in a local reference system) for each pin (hole's center). In particular, since the bearing loads are the most critical values for such a problem, the last ones have been defined as objective function while the axial loads have been set as constraint functions. Totally, 8 objective functions have been defined (4 for deployed configuration and 4 for folded configuration).

In order to better illustrate the optimization results, the output variables are reported for both folded and deployed configuration separately. Fig 15 reports the two bubble 4D graphs, one foreach configurations. The best designs, for both configurations, are concentrated in different regions of the domain. But it is possible to identify some configurations which are present in both graphs and which are able to return good results for both configurations.

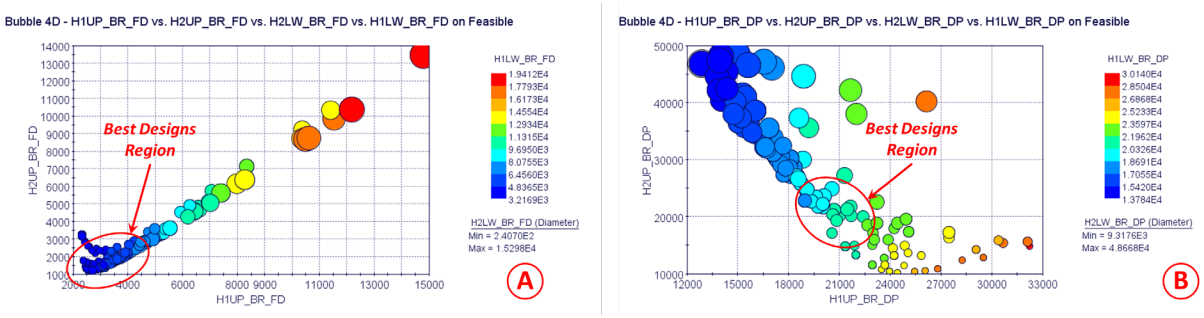


**Fig 15.** Bubble 4D graph for deployed (A) and folded (B) configuration

The results highlight that the objective functions are minimized as the relative distance between the two hinges increases. All selected designs provide bearing loads very close each other and therefore, the final choice could be done considering other functional requirements, such as the real possibility of installing the hinges in the selected regions. Such results have been used to preliminarily estimate the bolts/pins diameter and the thickness of the surrounding plates. Considering the mission that the vehicle has to perform, the operative environmental conditions lead to select the titanium alloy (Ti6Al4V) as the ideal material for such components. Considering an operative temperature equal to 160°, the shear ultimate stress is 398 MPa, the bearing stress is 1071 MPa and the ultimate tensile stress is 530 MPa.

In order to estimate the diameters and the thicknesses of the connection components, only the maximum loads coming from the best design sets, for each configuration (wing unfolded and folded), have been considered. Table 3 shows the minimum diameters of the locking pins and hinge rods, considering a Safety Factor equal to 1.5 and a number of cutting planes equal to 2.

**Table 3.** diameter of locking pins and bolts

| *Wing Configuration* | *Max Force [N]* | *Yield Stress [MPa]* | *SF* | *Shear Plane* | *Min Bolt Area [mm²]* | *Min Bolt Diameter [mm]* |
|---|---|---|---|---|---|---|
| Deployed | 23878.6 | 398.3 | 1.5 | 2 | 44.96 | 7.57 |
| Folded | 7449.1 | 398.3 | 1.5 | 2 | 14.03 | 4.23 |

Considering the determined bolts diameters, it is possible to evaluate the minimum thickness of the plates that should hold the holes and the pins for avoiding any bearing (Table 4) and net section failure (Table 5).

**Table 4.** minimum plate thickness for bearing sizing

| *Wing Configuration* | *Max Force [N]* | *Yied Bearing [MPa]* | *SF* | *Min Bolt Diameter [mm]* | *Plate Thickness [mm]* |
|---|---|---|---|---|---|
| Deployed | 23878.6 | 1071.8 | 1.5 | 7.57 | 4.42 |
| Folded | 7449.1 | 1071.8 | 1.5 | 4.23 | 2.47 |

**Table 5.** minimum plate thickness for net section failure

| *Wing Configuration* | *Max Force [N]* | *Yied Bearing [MPa]* | *SF* | *Min Bolt Diameter [mm]* | *Plate Thickness [mm]* |
|---|---|---|---|---|---|
| Deployed | 23878.6 | 530.6 | 1.5 | 7.57 | 8.92 |
| Folded | 7449.1 | 530.6 | 1.5 | 4.23 | 4.98 |

## 6. Thermal Protection System concept definition

Heat fluxes on the vehicle's critical areas have been computed on selected points along a reference trajectory taken from previous studies (USV3, IXV). These aerothermal loads have been used for preliminary sizing of thermal protection system. The aerothermal loads are obtained with fully catalytic assumptions that are very conservative when considering the use of C/SiC materials. Typical assumption for sizing design is a reduction of 30% from fully catalytic results. Recent experimental activities have shown a further lower catalysis efficiency [2]. The following simplified profile (orange line in figure 16) was considered for nose and wing leading edges TPS sizing of the new USV3 DWS configuration.

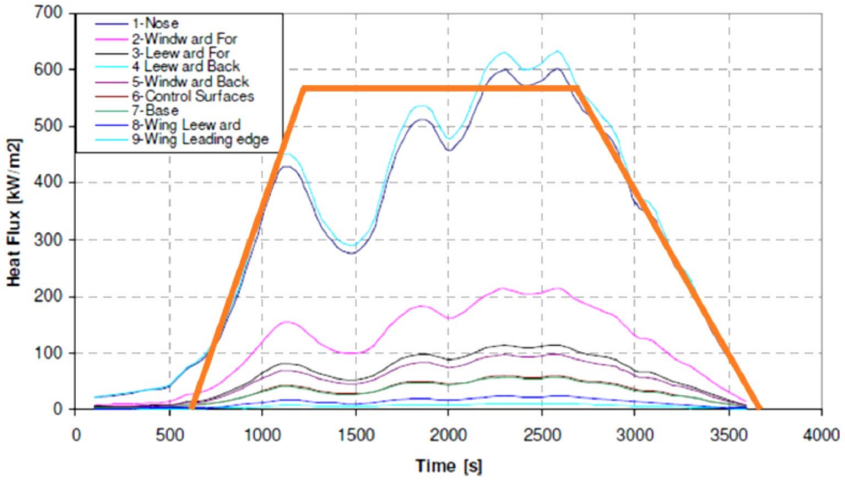


**Fig 16.** Considered Heat Flux Profiles

TPS preliminary sizing can be performed with the same approach and stack-up materials used for CIRA USV3 preliminary design [15] and IXV project [16], as reported in Table 6.

**Table 6.** TPS Preliminary Thickness

| Zone | Outer layer | 1st Insulation Layer | 2nd Insulation Layer | 3rd Insulation Layer |
|---|---|---|---|---|
| Nose | CMC (3mm) | Zircar (97,5 mm) | Pyrogel (15 mm) | |
| Windward | CMC (3mm) | Zircar (81 mm) | Aeroguard 12(mm) | Pyrogel (20 mm) |
| Hot Leeside | EI (40 mm) | Pyrogel (55 mm) (TBC) | - | - |
| Cold Leeside | EI (40-65 mm) (TBC) | - | - | - |

Some analyses were performed more in detail on the wing TPS considering the same CMC and insulation materials but a Titanium wing box instead of Aluminum honeycomb one (used for the cold structure of IXV). One-dimensional analysis has been performed consisting of a stuck of elements from outer surface (C/SiC) to inner structure (Ti6Al4V). Each material is characterized by its thermal properties.

Thermal loads are applied assuming radiative equilibrium temperature history along the re-entry trajectory on external skin. In particular, three points were selected on the wing leading edge and on wing windward. In order to identify the best possible configuration of insulation thickness an optimization process has been performed, assuming materials limits as constraints.

Assuming a Titanium cold structure of 2 mm, including the wing skin (1 mm), and the global effect of titanium stringers (1 mm), the thicknesses reported in Table 7 were obtained.

 

**Table 7.** Wing Hot Zone Preliminary Sizing

| Heat Flux | T ext. | Thickness [mm] | | | | MAX TEMP [°C] | | |
|---|---|---|---|---|---|---|---|---|
| [kW] | [°C] | Pyrogel | Aeroguard | Zircar | Totale | Pyrogel | Aeroguard | Cold S. |
| 560 | 1600 | 20 | 10 | 70 | 100 | 629,1 | 960,7 | 330,2 |
| 360 | 1400 | 10 | 2 | 70 | 82 | 455,6 | 551,3 | 364,0 |
| 200 | 1180 | 10 | 5 | 50 | 65 | 387,0 | 631,8 | 292,9 |

The total thickness of TPS on wing leading edges and windward is preliminary estimated varying from 100 to 65mm. On the leeside beyond the leading edges, considering the high thermal capacity of Titanium skin that reduces largely the radiative equilibrium temperature, no insulation is presently foreseen.

The TPS of USV3 DWS configuration follows the aerothermal loads on the aeroshape and preliminary sizing. Leading edges of fuselage and wings, together with all the windward area, are characterized by an external CMC thin layer of few millimeters and by different layers of insulators in order to reduce the high temperature on the external surface to acceptable limit for cold structures. Aerodynamic control surfaces, including rudders, ailerons and body-flap, will be designed as CMC hot structures. On the leeward flexible external insulator are foreseen. The TPS selected material layout is shown in Fig 17.

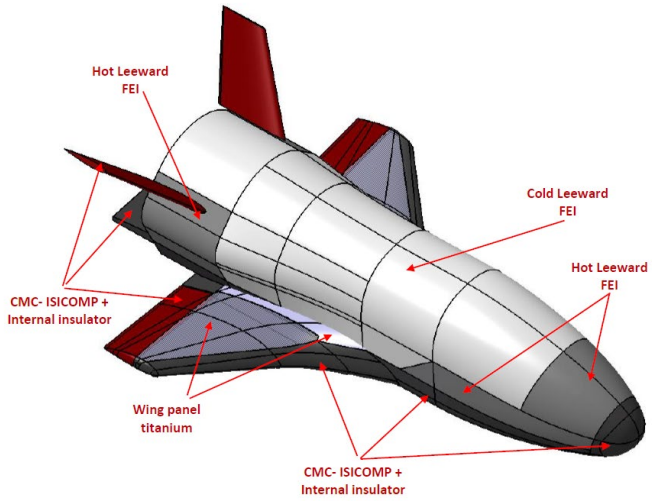


**Fig 17.** TPS Layout

## 7. Conclusions

A global overview about the activities performed in the framework of CIRA USV3 DWS project has been provided. Starting from initial trade-off studies, a "wing body based" concept has been selected and the baseline configuration has been defined. Complete aerodynamic and aerothermodynamic databases have been developed for hypersonic, supersonic, transonic and subsonic regimes, from Mach 25 down to landing. In agreement with the objectives of the USV3 DWS project, in terms of key technologies to be investigated, DWS and TPS sub-systems concept design has been defined, too.

The project activities have been concluded with the definition of the system preliminary requirements and the successful conclusion of the related USV3 DWS PRR milestone. Following development phases are foreseen to be completed in the next future.

## References

1. Tumino, G.; Mancuso, S.; Gallego, J.-M.; Dussy, S.; Preaud, J.-P.; Di Vita, G.; Brunner, P. The IXV experience, from the mission conception to the flight results. Acta Astronautica 2016, 124, 2–17.
2. M. De Stefano Fumo, G. Rufolo, R. Gardi, R. Fauci, A. De Fenza, F.M. Pisano, G.M. Infante, L. Cavalli, M. Valle: Design, Development and Testing of the CMC Thermal Protection System

 

and Body Flap Assembly of Space Rdier, the First Reusable European Space Transportation System. 2nd International Conference on Flight Vehicles, Aerothermodynamics and Re-entry Missions & Engineering (FAR) 19 - 23 June 2022. Heilbronn, Germany.

3. B.Galasso, R.Fauci: Preliminary trade-off study of deployment systems for USV3 unmanned space re-entry vehicle. XXV AIDAA International Congress Rome, Italy, 9-12 Sept. 2019.
4. M. De Stefano Fumo, A. Pugliese, G. Pezzella and G. Guidotti: Small Autonomous Winged Aeroshape Trade-off through Mission and System Guidelines. 65th International Astronautical Congress, Toronto, 2014.
5. Capizzano, F., Catalano, P., Marongiu, C., and Vitagliano, P. L., "U-RANS Modelling of Turbulent Flows Controlled by Synthetic Jets", 35th AIAA Fluid Dynamics Conference, Toronto, June 6-9 2005, AIAA paper 2005-5015.
6. Catalano, P. and Tognaccini, R., "Turbulence modelling for low Reynolds number flows", AIAA Journal, Vol. 48, 2010, pp. 1673-1685.
7. Catalano, P., Mele, B., and Tognaccini, R., "On the implementation of a turbulence model for low Reynolds number flows", Computers and Fluids, Vol. 109, March 2015, pp. 67-71.
8. Gary R. Saaris, "A502I User's Manual-PAN AIR Technology Program for Solving Problems of Potential Flow about Arbitrary Configurations", Boeing D6-54703, 02-1992.
9. "Viscous Effects on Complex Configurations". Software User's Manual, WL-TR-95-3060, August 1995.
10. Schlichting, H., Gersten, K., "Boundary Layer Theory", 8th ed. Springer-Verlag 2004, ISBN 81-8128-121-7.
11. Christian Lupo, Brandan Robertson and George Gafka, "The X-38 V-201 Fin Fold Actuation Mechanism", 37th Aerospace Mechanisms Symposium, Johnson Space Center, May 19-21, 2004.
12. F. Di Caprio, R. Scigliano, R. Fauci, D. Tescione, "Design Optimization of Interfacing Attachments for the Deployable Wing of an Unmanned Re-Entry Vehicle", Algorithms 2021, 14, 141.
13. Roland LAGIER. Vega C User's Manual by Arianespace Group. Available online: https://www.arianespace.com/wp-content/ uploads/2018/07/Vega-C-user-manual-Issue-0-Revision-0_20180705.pdf (accessed on 28 July 2022).
14. Mode-Frontier Esteco. User manual. Available online: https://www.esteco.com/modefrontier (accessed on 28 July 2022).
15. M. De Stefano Fumo, G. Guidotti, C. Richiello, "USV3 System Concept Development Overview", Aerotec. Missili Spaz. 93, 25–32 (2014). https://doi.org/10.1007/BF03404673.
16. E. Brach Prever, M. T. Signorelli, F. Camarri, A. Denaro, G. Di Vita, "TPS Design, Development and Verification Approach for IXV Program", 7th European Workshop on TPS&HS Apr. 8-10, 2013.

 